^{18}F-FDG Kinetics in Locally Advanced Breast Cancer: Correlation with Tumor Blood Flow and Changes in Response to Neoadjuvant Chemotherapy

Jeffrey Tseng, MD; Lisa K. Dunnwald, BS; Erin K. Schubert, BA; Jeanne M. Link, PhD; Satoshi Minoshima, MD, PhD; Mark Muzi, MS; and David A. Mankoff, MD, PhD

Division of Nuclear Medicine, Department of Radiology, University of Washington, Seattle, Washington

The aim of this study was to characterize the biologic response of locally advanced breast cancer (LABC) to chemotherapy using ^{15}O-water–derived blood flow measurements and ^{18}F-FDG–derived glucose metabolism rate parameters. **Methods:** Thirty-five LABC patients underwent PET with ^{15}O-water and ^{18}F-FDG before neoadjuvant chemotherapy and 2 mo after the initiation of treatment. Kinetic analysis for ^{15}O-water was performed using a single tissue compartment model to calculate blood flow; a 2-tissue compartment model was used to estimate ^{18}F-FDG rate parameters K_1, k_2, k_3, and the flux constant, K_i. Correlations and ratios between blood flow and ^{18}F-FDG rate parameters were calculated and compared with pathologic tumor response. **Results:** Although blood flow and ^{18}F-FDG transport (K_1) were correlated before chemotherapy, there was relatively poor correlation between blood flow and the phosphorylation constant (k_3) or the overall ^{18}F-FDG flux (K_i). Blood flow and ^{18}F-FDG flux were more closely matched after chemotherapy, with changes in k_3 accounting for the increased correlation. These findings were consistent with a decline in both the K_i/flow and k_3/flow ratios with therapy. The ratio of ^{18}F-FDG flux to transport (K_i/K_1) after 2 mo of chemotherapy was predictive of ultimate response. **Conclusion:** The pattern of tumor glucose metabolism in LABC, as reflected by analysis of ^{18}F-FDG rate parameters, changes after therapy, even in patients with modest clinical responses. This may indicate a change in tumor "metabolic phenotype" in response to treatment. A low ratio of glucose metabolism (reflected by K_i) to glucose delivery (reflected by K_1 and blood flow) after therapy is associated with a favorable response. Further work is needed to understand the tumor biology underlying these findings.

Key Words: ^{18}F-FDG; ^{15}O-water; blood flow; kinetic analysis; breast cancer; tumor biology; response to therapy; PET

J Nucl Med 2004; 45:1829–1837

Locally advanced breast cancer (LABC) is defined as a large primary tumor (T3 or greater) or advanced axillary disease (N2) without evidence of distant metastases (*1*). These tumors are frequently treated using primary or neoadjuvant chemotherapy before definitive surgery (*2*). Prior studies have suggested that serial measurements of tumor glucose metabolism using ^{18}F-FDG PET are helpful for monitoring tumor response (*3–7*).

We have studied LABC response using serial dynamic ^{15}O-water and ^{18}F-FDG scans to investigate how tumor blood flow and glucose metabolism change after presurgical neoadjuvant chemotherapy. Our previous results have shown that high glucose metabolism or an imbalance between blood flow and glucose metabolism before chemotherapy predict a poor response to neoadjuvant chemotherapy (*8*). We have also shown that changes in blood flow after 2 mo of treatment predict response to chemotherapy: Responders have a decrease in tumor blood flow, whereas nonresponders have an increase in tumor blood flow (*9*).

We now extend our prior work to include a more detailed analysis of glucose metabolism and its relationship to blood flow using a 2-tissue compartmental model for ^{18}F-FDG (*10*). Similar work has been presented by Zasadny et al. (*11*), who performed kinetic analysis of ^{18}F-FDG in 9 untreated breast cancers patients. Their study showed a positive correlation between blood flow and glucose metabolism and provided insights into the pattern of glucose metabolism in untreated LABC. The authors suggested that areas of the tumor with low blood flow and high metabolism might be hypoxic. This is consistent with prior invasive studies that showed hypoxic areas heterogeneously distributed within some LABC (*12*) and with our prior work showing that high glucose metabolism and low blood flow predicts a less favorable response to treatment (*8*).

In this article we report the kinetic analysis of glucose metabolism in a series of 35 patients who had both ^{15}O-water and ^{18}F-FDG PET studies before and 2 mo after the

Received Feb. 8, 2004; revision accepted May 21, 2004.

For correspondence or reprints contact: David A. Mankoff, MD, PhD, Division of Nuclear Medicine, Box 356113, University of Washington Medical Center, 1959 N.E. Pacific St., Seattle, WA 98195-6113.

E-mail: dam@u.washington.edu

initiation of neoadjuvant chemotherapy. This report differs from previous studies in the size of the patient population and the inclusion of measurements both before and after chemotherapy. The aim of the study was to characterize the relationship among the individual ^{18}F-FDG rate parameters, compared with ^{15}O-water–derived blood flow and to pathologic macroscopic response to neoadjuvant chemotherapy. Our hypothesis is that changes in the pattern of tumor metabolism, including the relationship between substrate utilization and delivery, will elucidate tumor biology and suggest factors important in resistance or response of LABC to chemotherapy.

METHODS AND MATERIALS

Patient Characteristics, Treatment, and Response Evaluation

Thirty-five LABC patients underwent serial ^{15}O-water and ^{18}F-FDG PET studies according to the University of Washington Human Subjects Committee guidelines. These 35 patients are the same patients who have been previously described (*9*); this work is a more detailed analysis of these previously reported imaging studies. Our patient selection criteria, chemotherapy regimen, and response evaluation have been previously described (*9*) and are summarized below and in the Results.

Patients underwent approximately 4 mo of neoadjuvant chemotherapy before surgery and lymph node dissection. Postchemotherapy surgical excision tumor samples were classified for tumor type and were graded for pathologic response to neoadjuvant chemotherapy by standard definitions (*13*) as in our prior studies (*9*). A macroscopic complete response (mCR) was defined as absence of macroscopic tumor by histopathologic examination. Patients with a residual mass and with a >50% reduction in size compared with prechemotherapy clinical size measurements based on ultrasound, mammography, or physical examination were considered a partial response (PR). The remaining patients were classified as no response (NR).

PET

Our radiopharmaceutical production methods and PET acquisition parameters have been described (*8,9*) and are summarized briefly here. PET images were obtained on an Advance Tomograph (General Electric Medical Systems) with 35 transaxial planes, 4.25-mm thick. Images were corrected for random coincidences, scatter, and attenuation. Filtered backprojection reconstruction was performed with a Hanning filter using a 35 × 128 × 128 image matrix and yielded a reconstructed spatial resolution of approximately 10–12 mm (*14*). Imaging was performed with 960–2,000 MBq (26–54 mCi) of ^{15}O-water and a 2-min infusion of 260–407 MBq (7–11 mCi) of ^{18}F-FDG. Glucose concentrations were checked immediately before the administration of ^{18}F-FDG (mean, 93 mg/dL; range, 60–170 mg/dL). Dynamic images were obtained for 7.75 min for ^{15}O-water and 60 min for ^{18}F-FDG. The dynamic imaging sequence for ^{15}O-water was 15 × 2 s, 15 × 5 s, 12 × 10 s, 8 × 15 s, and 6 × 20 s. The imaging sequence for ^{18}F-FDG was 4 × 20 s, 4 × 40 s, 4 × 1 min, 4 × 3 min, and 8 × 5 min.

Tumor regions of interest (ROIs) were drawn as 1.5-cm-diameter circles on the ^{18}F-FDG images around the area of maximum tumor activity over 3 contiguous planes chosen to be the most biologically aggressive portion of the tumor. The choice of circular 1.5-cm ROIs was a compromise between selecting regions of sufficient size and counts for analysis and more severe partial-volume (PV) effects for larger regions. These ROIs were copied onto the ^{15}O-water scans. ROIs were drawn within the left ventricular cavity—close to the valve plane to avoid spillover from adjacent myocardium—to provide a blood input function. ROIs were also drawn around the contralateral breast to serve as background. Images were obtained before neoadjuvant chemotherapy (mean, 4.1 d; range, 0–12 d) and approximately 2 mo after the initiation of chemotherapy (mean, 9.3 wk; range, 6–15 wk). The mean duration of chemotherapy was 14.4 wk (range, 8–24 wk).

Kinetic Models

The ^{15}O-water analysis used a single tissue compartment model described by the following differential equation according to Wilson et al. (*15*):

$$\frac{dA(t)}{dt} = F \cdot C_b(t) - (F/V_d + \lambda) \cdot A(t), \qquad \text{Eq. 1}$$

where A(t) is the tissue activity, $C_b(t)$ is the blood activity, F is blood flow, V_d is the volume of distribution, and λ is the radioactive decay constant for ^{15}O.

The ^{18}F-FDG analysis used a 2-tissue compartment model described by the following differential equations, which were modified from Sokoloff et al. (*10*) to incorporate decay of the radiotracer:

$$\frac{dC_{FDG}(t)}{dt} = K_1 \cdot C_b(t) - (k_2 + k_3 + \lambda) \cdot C_{FDG}(t), \qquad \text{Eq. 2}$$

$$\frac{dC_{FDG-P}(t)}{dt} = k_3 \cdot C_{FDG}(t) - \lambda \cdot C_{FDG-P}(t), \qquad \text{Eq. 3}$$

where $C_{FDG}(t)$ is the free ^{18}F-FDG tissue activity, $C_{FDG-P}(t)$ is the phosphorylated ^{18}F-FDG tissue activity, C_b is the blood activity, K_1 is the ^{18}F-FDG transport rate constant from blood to tissue, k_2 is the ^{18}F-FDG transport rate constant from tissue to blood, k_3 is the phosphorylation rate constant of ^{18}F-FDG, and λ is the radioactive decay constant for ^{18}F. The overall flux constant, K_i, is represented by the following equation:

$$K_i = \frac{K_1 \cdot k_3}{k_2 + k_3}. \qquad \text{Eq. 4}$$

In addition to K_1, k_2, k_3, and K_i, we also calculated the K_i/K_1 ratio. This ratio K_i/K_1 is equivalent to $k_3/(k_2 + k_3)$ and reflects the balance between ^{18}F-FDG delivery to tissue (K_1) and ^{18}F-FDG phosphorylation (k_3) (*16*). Ratios close to 0 suggest that the flux constant K_i is limited by the phosphorylation step. Ratios close to 1 suggest that ^{18}F-FDG delivery K_1 is rate limiting.

For the ^{18}F-FDG model, tissue time–activity curves are the sum of the C_{FDG} and C_{FDG-P} compartments and a small contribution from the intravascular blood volume. For the ^{18}F-FDG analysis, a $BV \cdot C_b(t)$ term was added to the tissue ROI, where BV is the percentage of intravascular blood volume in the tissue. We fixed BV at 4% based on literature values for breast tumors (*17–19*). Simulations showed that 2-fold changes in BV did not significantly change the ^{18}F-FDG parameters, K_1, k_2, and k_3. For the ^{15}O-water model, we followed the convention of Wilson et al. (*15*) and ignored the small intravascular volume. Simulations showed that blood volume could not be estimated accurately from the ^{15}O-

water data, and an attempt to estimate blood volume in the ^{15}O-water study analysis increased variability of the flow estimates.

Parameter estimation via optimization was performed using Berkeley Madonna software. During optimization, parameters were constrained to a range of 0 to 1 (mL/min/g for blood flow, K_i, and K_i; min^{-1} for k_2 and k_3) with the exception of k_3, which had a lower constraint of 0.0001 min^{-1}. Parameter accuracy was estimated by simulations with statistical noise added to match the levels observed in clinical studies. For ^{15}O-water, the 1-min time point had a coefficient of variation of 7.5%. For ^{18}F-FDG, the 10-min time point had a 3.6% coefficient of variation. Simulations suggested a typical SE of 13% for blood flow, 11% for K_1, 23% for k_2, 21% for k_3, and 3% for K_i. Using Kinetic Imaging System software, the mean SEs for the individual patient's parameters were estimated as 16% for blood flow, 11% for K_1, 22% for k_2, and 25% for k_3, which were in close agreement with the simulations.

Flux constants estimated by compartmental analysis were compared with previously reported K_i estimates from Patlak graphical analysis (*9*). The flux constants estimated for these 2 methods were nearly identical (graphical K_i vs. compartment K_i, $r = 0.98$).

PV Correction

To account for effects of changes in tumor size on parameter estimates, imaging data were also corrected for PV effects as described previously (*9,20*). Tumor size was assessed by ultrasound, mammography, or physical examinations within 1 wk of PET. Prior studies in our tomograph have shown that PV correction is necessary for tumors <3 cm (*20*). This was the case for 6 tumors before chemotherapy (4 mCR and 2 PR) and 15 tumors after chemotherapy (7 mCR and 8 PR). PV correction was performed as has been previously described (*9,20*):

$$A'(t) = \frac{A(t) - Bkgd(t)}{RC} + Bkgd(t), \qquad \text{Eq. 5}$$

where $A'(t)$ is the PV-corrected tumor activity, $A(t)$ is the uncorrected tumor activity, $Bkgd(t)$ is the background activity obtained from an ROI from the contralateral breast, and RC is the recovery coefficient measured using phantom studies (*20*).

Statistical Analysis

The means and SDs were determined for the ^{18}F-FDG parameters, K_1, k_3, and K_i, for each of the pathologic groups, mCR, PR, and NR, before and after chemotherapy. Since k_2 can be derived from K_1, k_3, and K_i, this parameter was not included in the reported results. Differences between the parameters before and after chemotherapy were tested for significance ($P < 0.05$) using the 2-tailed paired Student *t* test and retested with the Wilcoxon matched-pairs signed-ranks test.

Correlations between blood flow and the ^{18}F-FDG rate parameters were calculated using the Pearson correlation coefficient. To minimize the effects of one far outlier with unusually high blood flow and metabolism, we excluded this patient from subsequent Pearson correlation coefficient analyses. All patients were included in an analysis with the nonparametric rank correlation test, Spearman ρ, which was performed to minimize the influence of the outlier. Differences in correlations before and after chemotherapy were assessed by performing a Fischer transformation on the correlation coefficients to obtain a *z*-score and then assessed for significance using a *t* test (*21*).

To evaluate whether the parameter estimates were influenced by the decreasing size of the lesion, PV corrections were applied, and the correlations were reassessed. In addition, ratios of the ^{18}F-FDG rate parameters to blood flow were calculated to minimize the influence of PV effects, since both terms in the ratio are affected similarly by partial volume. Ratios before and after chemotherapy were compared using the 2-tailed paired Student *t* test and retested with the Wilcoxon matched-pairs signed-ranks test.

Differences among the pathologic response groups' K_i/flow and K_i/K_1 ratios after chemotherapy were tested for significance using the nonparametric Kruskal–Wallis test (*21*). Since both K_i and K_1 can be influenced by plasma glucose concentrations, glucose correction was applied to K_i and K_1 by multiplying the terms by the plasma glucose concentration and then retested for significance. Glucose correction was also used to retest significance when comparing the parameters before and after chemotherapy. Statistical analyses were performed using JMP software (SAS Institute).

4-Parameter ^{18}F-FDG Model

The ^{18}F-FDG model described above has 3 parameters, K_1, k_2, and k_3 (3-parameter model) and assumes that there is no appreciable dephosphorylation of ^{18}F-FDG-6-phosphate—that is, $k_4 = 0$. To test the effect of dephosphorylation on our results, we tested an additional model that incorporated a k_4 term (4-parameter model) as described by Phelps et al. (*22*). An upper bound of 0.03 min^{-1} was placed on the k_4 term based on literature values (*23–27*). This model was used to determine the effect of including a k_4 parameter on the estimates of the remaining parameters, K_1, k_2, k_3, and K_i and for changes in the significance levels for the above tests.

RESULTS

Patient Characteristics, Treatment, and Response Evaluation

The patient characteristics have been previously described (*9*) and are summarized here. The mean patient age was 49 y (range, 32–76 y). The mean primary tumor size was 5.5 cm (range, 1.9–11.0 cm). The chemotherapy regimen consisted of a combination of weekly dose-intensive doxorubicin with granulocyte colony-stimulating factor support for 32 patients; 28 of 32 also had cyclophosphamide and 2 of 32 patients also had cyclophosphamide and fluorouracil. For the remaining 3 patients, 1 had 3-wk cycles of docetaxel and vinorelbine, 1 had cyclophosphamide/methotrexate/fluorouracil and concurrent radiation, and 1 had weekly palitaxel and trastuzumab.

Tumors were classified as infiltrating ductal carcinoma in 32 patients and infiltrating lobular carcinoma in 3 patients. A mCR was achieved in 14 of 35 patients, PR in 16 of 35 patients, and NR in 5 of 35 patients.

^{18}F-FDG Rate Parameters Before and After Chemotherapy

The ^{18}F-FDG parameters K_1, k_2, k_3, and K_i before neoadjuvant chemotherapy (prechemotherapy) and after approximately 2 mo of chemotherapy (postchemotherapy) are shown in Table 1. For all parameters, the mean value of the rate constant decreased significantly after therapy when including all patients ($P < 0.001$). PV correction did not alter the significance of these results.

TABLE 1
^{18}F-FDG Kinetic Parameters Before and After Chemotherapy for Response Groups

Parameter	Group	Before chemo (mean ± SD)	After chemo (mean ± SD)	*t* test *P* value
K_i*	mCR	0.018 ± 0.015	0.0026 ± 0.0027	<0.01
	PR	0.017 ± 0.010	0.0061 ± 0.0042	<0.001
	NR	0.035 ± 0.024	0.026 ± 0.020	0.03
	All	0.020 ± 0.015	0.008 ± 0.011	<0.001
K_1*	mCR	0.14 ± 0.05	0.052 ± 0.029	<0.001
	PR	0.13 ± 0.06	0.087 ± 0.040	0.02
	NR	0.16 ± 0.04	0.19 ± 0.10	0.52
	All	0.14 ± 0.05	0.09 ± 0.06	<0.001
k_3†	mCR	0.038 ± 0.029	0.0064 ± 0.0062	<0.01
	PR	0.043 ± 0.022	0.016 ± 0.009	<0.001
	NR	0.073 ± 0.045	0.048 ± 0.037	0.02
	All	0.046 ± 0.030	0.017 ± 0.020	<0.001
K_i (PV corrected)	mCR	0.019 ± 0.014	0.0036 ± 0.0033	<0.01
	PR	0.017 ± 0.010	0.0068 ± 0.0054	<0.001
	NR	0.035 ± 0.024	0.026 ± 0.020	0.03
	All	0.020 ± 0.015	0.008 ± 0.011	<0.001
K_1 (PV corrected)	mCR	0.16 ± 0.05	0.073 ± 0.034	<0.001
	PR	0.13 ± 0.06	0.12 ± 0.06	0.44
	NR	0.16 ± 0.04	0.19 ± 0.10	0.52
	All	0.14 ± 0.06	0.11 ± 0.07	<0.001
k_3 (PV corrected)	mCR	0.040 ± 0.033	0.0063 ± 0.0062	<0.01
	PR	0.044 ± 0.022	0.015 ± 0.012	<0.001
	NR	0.073 ± 0.045	0.048 ± 0.037	0.02
	All	0.046 ± 0.032	0.016 ± 0.021	<0.001

*mL/min/g.
†min^{-1}.
chemo = chemotherapy.

Data for the individual response groups mCR, PR, and NR are also presented in Table 1. After chemotherapy, mean K_1 declined in the mCR and PR groups, whereas it increased in the NR group. This pattern was also seen for blood flow, as reported previously (*9*). Mean K_i and k_3 parameters decreased for all groups, with the largest declines occurring in the mCR group and the smallest declines occurring in the NR group. K_i also declined after therapy in all patients except 1 patient who had very low uptake before therapy, making the small increase after therapy difficult to interpret. Retesting the significance levels using the nonparametric Wilcoxon matched-pairs signed-ranks test showed similar significance levels except for the NR group for K_i and k_3, which showed a trend toward significance ($P = 0.06$). PV correction did not affect the significance levels. A summary graph showing the mean blood flow and K_i changes before and after chemotherapy for the mCR, PR, and NR groups is shown with SEMs (Fig. 1).

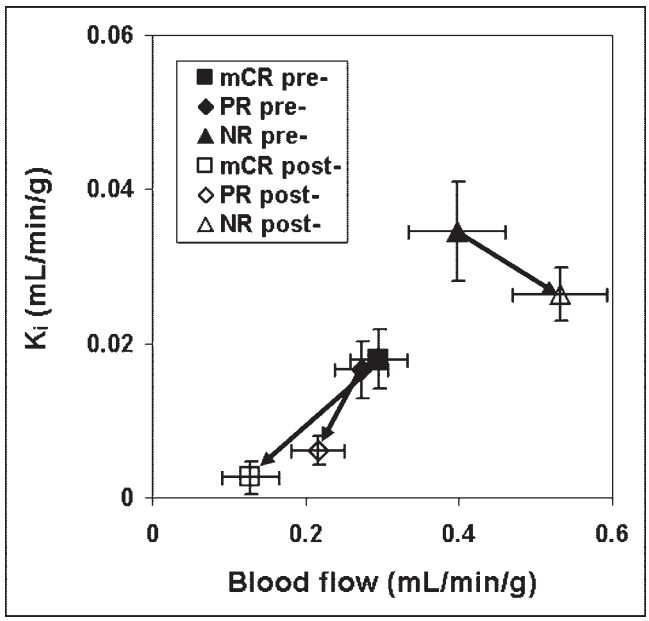

FIGURE 1. Arrows show direction of changes in mean blood flow and K_i values before → after chemotherapy. K_i decreased for all response groups. Blood flow decreased for mCR and PR groups; however, it increased for NR group. Error bars represent SEM.

Correlations Between Blood Flow and ^{18}F-FDG Parameters

Correlations between blood flow and K_1, k_3, or K_i before and after chemotherapy were tested using the Pearson correlation coefficient. Before chemotherapy, the correlation coefficient between blood flow and K_i was 0.60 (Fig. 2);

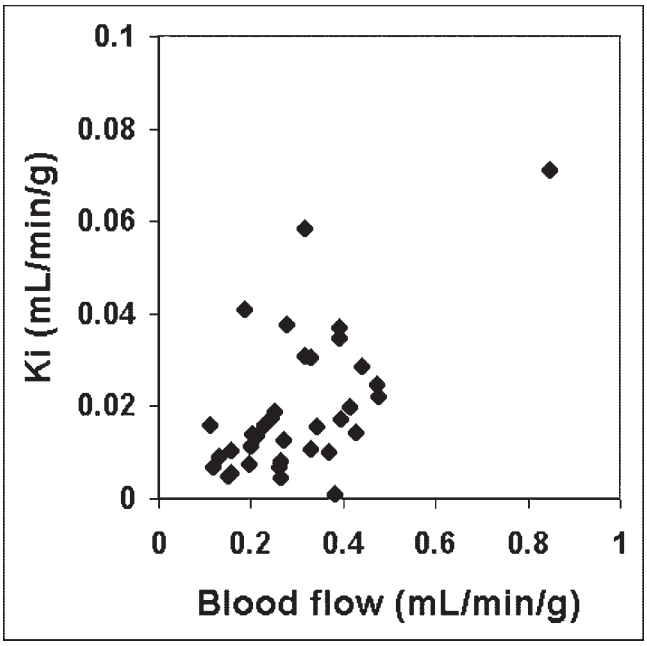

FIGURE 2. Correlation between blood flow and K_i before chemotherapy for all patients revealed 1 far outlier.

however, there was 1 outlying patient, which artificially elevated the correlation. After removing the outlier from all subsequent analyses (Table 2, upper half), the correlation between blood flow and K_i was much poorer ($r = 0.34$, $P = 0.05$). With the outlier excluded, a moderately strong correlation between blood flow and K_1 persisted ($r = 0.62$, $P < 0.001$). There was no significant correlation between blood flow and k_3 ($r = 0.11$, $P = 0.52$).

After chemotherapy, the correlations were stronger between blood flow and K_i ($r = 0.76$) and k_3 ($r = 0.66$), whereas the correlation between blood flow and K_1, which was already moderately strong, improved only slightly ($r = 0.81$). Analyses with the nonparametric rank correlation test, Spearman ρ, revealed similar correlations and significance levels (Table 2, lower half). Representative graphs for the correlations between blood flow and K_i or K_1 before and after chemotherapy are shown (Figs. 3A–3D).

The *P* values for the difference in correlation coefficient before and after chemotherapy are given on the right side of Table 2. The correlation coefficient for blood flow versus K_1 did not show a significant change, whereas the correlation coefficients for blood flow versus K_i and blood flow versus k_3 showed significant differences ($P = 0.01$ for both).

With PV corrections, correlations between blood flow versus K_i and blood flow versus k_3 were somewhat poorer after chemotherapy, and before and after differences were no longer significant; however, the trends remained.

Ratios of ^{18}F-FDG Parameters to Blood Flow

The relationship between blood flow and the ^{18}F-FDG parameters were also examined using ratios to minimize the influence of PV effects. Ratios of the ^{18}F-FDG parameters to blood flow before and after chemotherapy are shown in Table 3. The ratios showed a significant decline in the K_i/flow ratio ($P < 0.001$) and the k_3/flow ratio ($P < 0.001$) after chemotherapy, but not for the K_1/flow ratio ($P = 0.11$).

Since blood flow is highly correlated with K_1, we also assessed the K_i/K_1 ratio after chemotherapy. Similar to the K_i/flow ratio, there was a significant decline for the K_i/K_1 ratio before to after chemotherapy ($P < 0.001$). PV correc-

TABLE 2
Correlations Between Blood Flow and ^{18}F-FDG Kinetic Parameters Before and After Chemotherapy

Parameter	Before chemo	*P* value	After chemo	*P* value	Before vs. after *P* value
			Pearson correlation coefficient* ($n = 34$)		
Flow and K_i	0.34	0.05	0.76	<0.001	0.01
Flow and K_1	0.62	<0.001	0.81	<0.001	0.11
Flow and k_3	0.11	0.52	0.66	<0.001	0.01
Flow and K_i (PV corrected)	0.28	0.10	0.62	<0.001	0.09
Flow and K_1 (PV corrected)	0.56	<0.001	0.69	<0.001	0.40
Flow and k_3 (PV corrected)	0.17	0.34	0.47	<0.01	0.18
			Spearman's ρ ($n = 35$)		
Flow and K_i	0.48	<0.01	0.74	<0.001	0.09
Flow and K_1	0.70	<0.001	0.82	<0.001	0.27
Flow and k_3	0.18	0.31	0.71	<0.001	<0.01
Flow and K_i (PV corrected)	0.29	0.02	0.44	<0.001	0.49
Flow and K_1 (PV corrected)	0.48	<0.001	0.52	<0.001	0.83
Flow and k_3 (PV corrected)	0.09	0.45	0.42	<0.001	0.15

*Far outlier removed.
chemo = chemotherapy.

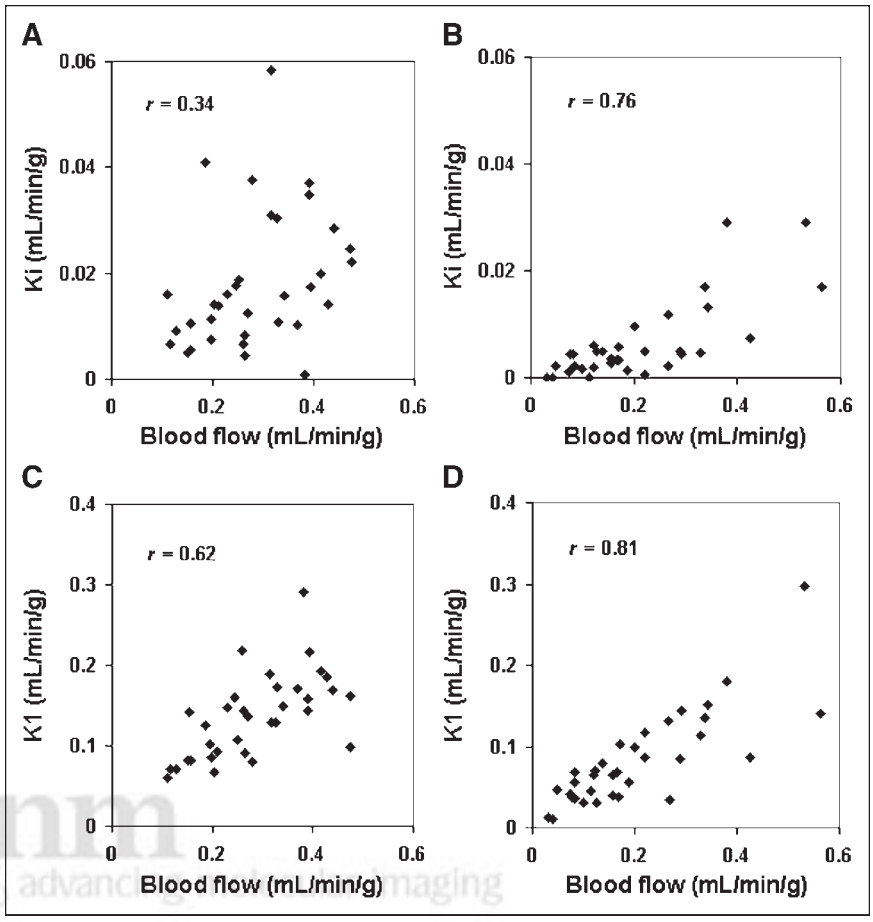

FIGURE 3. Correlations between blood flow and K_i or K_1 before and after chemotherapy excluding 1 far outlier. (A) Blood flow and K_i before chemotherapy. (B) Blood flow and K_i after chemotherapy. (C) Blood flow and K_1 before chemotherapy. (D) Blood flow and K_1 after chemotherapy. Correlation between blood flow and K_i improved after chemotherapy.

tion did not change the significance of these results. Retesting the significance levels using the Wilcoxon matched-pairs signed-ranks test showed similar results.

K_i/Flow and K_i/K_1 Versus Response After Chemotherapy

The K_i/flow ratio is analogous to the metabolic rate of ^{18}F-FDG (MRFDG)/flow ratio presented in our previous work (*8*), which was predictive of macroscopic response for the values before chemotherapy. In the current analysis, the ratios after chemotherapy for K_i/flow showed a trend for significant differences among the response groups (Table 4), with mean ratios of mCR = 0.020, PR = 0.031, and NR = 0.045 (P = 0.09). However, the trend was lost with PV correction. The K_i/flow ratio for the mCR group approached values seen for normal contralateral breast (0.016).

TABLE 3
^{18}F-FDG Parameters to Blood Flow Ratios Before and After Chemotherapy

Ratio	Before chemo (mean ± SD)	After chemo (mean ± SD)	*t* test *P* value
K_i/flow	0.068 ± 0.046	0.028 ± 0.019	<0.001
K_1/flow	0.50 ± 0.15	0.43 ± 0.17	0.11
k_3/flow	0.18 ± 0.15	0.069 ± 0.047	<0.001
K_i/K_1	0.15 ± 0.11	0.069 ± 0.048	<0.001
K_i/flow (PV corrected)	0.068 ± 0.046	0.031 ± 0.024	<0.001
K_1/flow (PV corrected)	0.50 ± 0.16	0.53 ± 0.40	0.70
k_3/flow (PV corrected)	0.17 ± 0.14	0.063 ± 0.054	<0.001
K_i/K_1 (PV corrected)	0.15 ± 0.11	0.062 ± 0.047	<0.001
K_i/flow (normal breast)	0.020 ± 0.022	0.016 ± 0.021	0.34
K_i/K_1 (normal breast)	0.053 ± 0.047	0.039 ± 0.043	0.17

chemo = chemotherapy.

TABLE 4
Ratios for Response Groups After Chemotherapy

Ratio	mCR (mean ± SD)	PR (mean ± SD)	NR (mean ± SD)	*P* value
K_i/flow	0.020 ± 0.016	0.031 ± 0.016	0.045 ± 0.027	0.08
K_i/K_1	0.044 ± 0.032	0.074 ± 0.038	0.12 ± 0.07	0.03
K_i/flow (PV corrected)	0.030 ± 0.029	0.027 ± 0.018	0.045 ± 0.027	0.44
K_i/K_1 (PV corrected)	0.042 ± 0.032	0.060 ± 0.035	0.12 ± 0.07	0.04

We also tested the K_i/K_1 ratios and found a significant difference among the response groups after chemotherapy (Table 4), with mean K_i/K_1 ratios of mCR = 0.044, PR = 0.074, and NR = 0.12 ($P < 0.01$). The mCR group, which had the lowest ratio, decreased to a value close to that of the normal contralateral breast (0.039). Repeat analysis of the ratios with PV-corrected data showed that the relationship to response remained significant ($P = 0.04$).

Testing Effect of a k_4 Model

By adding a k_4 term in the compartment models, k_4 was estimated as a mean of 0.014 ± 0.012 min^{-1} before chemotherapy and 0.019 ± 0.022 min^{-1} after chemotherapy. Using the 4-parameter model, the rate parameters K_1, k_2, and k_3 and K_i increased on average by 11%, 40%, 77%, and 41%, respectively. This is expected as a result of the effects of a k_4 term (*28*). Recalculating the *P* values for Tables 1, 3, and 4 did not change the significance for any of the comparisons for the 4-parameter model versus the 3-parameter model. In addition, glucose correction also did not change the significance for any of the comparisons in Tables 1, 3, and 4.

DISCUSSION

This study is a more in-depth analysis of dynamic image data previously reported for LABC patients studied with ^{18}F-FDG and ^{15}O-water PET both before and after chemotherapy using a more detailed analysis of ^{18}F-FDG kinetics. In this more rigorous kinetic analysis, we found that glucose blood-to-tissue transport (K_1) correlated with blood flow, but blood flow and glucose metabolism (K_i) in LABC were not necessarily matched before chemotherapy. This is in distinction to what has been reported for normal tissues such as the heart and brain, where tissue glucose metabolism and blood flow are tightly coupled (*29,30*). In our series, tumor glucose metabolism and blood flow changed differently after chemotherapy, and they became more tightly correlated. The ratio of glucose metabolism to blood flow decreased for all tumors. In more responsive tumors, the ratios decreased to values close to those of the normal breast.

Kinetic analysis suggests that the phosphorylation step (k_3) is responsible for the changes before and after chemotherapy. Both k_3 and the k_3/flow ratio had significant declines after therapy. In contrast, K_1 and K_1/flow showed no significant changes. These findings are in agreement with Torizuka et al., who suggested that k_3 is the rate-limiting factor in ^{18}F-FDG accumulation in untreated breast cancers rather than K_1, which reflects glucose delivery (*31*). In our series, we found that as chemotherapy slowed tumor growth and reduced the overall tumor burden, glucose metabolism declined, on the average, more than blood flow. The result was a closer match between metabolism and blood flow after therapy, nearer to the metabolism/blood flow ratio seen in normal breast. Thus, there was a shift in the ^{18}F-FDG kinetic pattern after chemotherapy, driven by the rate of phosphorylation (k_3) relative to glucose delivery (K_1).

A possible explanation for these findings is tumor hypoxia in some tumors before therapy. Tumor hypoxia has been shown to induce cellular changes, including increased expression of glycolytic enzymes, increased angiogenesis signals, and altered cell cycling (*32*). Under these conditions, there is more anaerobic metabolism through glycolysis, which may lead to resistance to apoptosis (*33*), culminating in malignant progression (*12*). Another intriguing possibility suggested by recent in vitro studies (*34*) is that altered glucose metabolism is a downstream consequence of altered cell survival signals and is, therefore, intimately associated with resistance to apoptosis.

Resolution of hypoxia or oxidative stress with treatment might be expected to return glucose metabolism to a state closer to that of the normal tissue. In our analysis, even in cases of minimal apparent response, chemotherapy led to altered ^{18}F-FDG kinetics with a shift closer to metabolic patterns seen in aerobic, nontumorous states. The best responding tumors had declines in the ^{18}F-FDG flux-transport ratio (K_i/K_1) to values close to those of the normal breast. This may help explain the decline in MRFDG with treatment, even in patients with minimal apparent tumor response (*9*).

In our study, we accounted for several factors that could lead to bias and could artificially increase the correlations between parameters—namely, PV effects, ^{18}F-FDG-6-phosphate dephosphorylation, and varying glucose concentrations. Of these factors, PV effects were the most dramatic and PV corrections reduced the correlations between blood flow and K_i, K_1, or k_3. PV correction itself can lead to errors since the correlation with radiographic or clinical size measurements can be inexact; therefore, PV correction can introduce additional variability in the corrected parameters. The trends for the changes before and after chemotherapy in correlations between blood flow and K_i, K_1, or k_3 persisted

after PV correction, suggesting that the change before and after therapy was not simply due to PV effects. Analysis of the ratios between ^{18}F-FDG parameters and blood flow circumvented most of the potential confounding effects of partial volume and supported the results of the correlation analyses.

Limitations in our analyses include the potential influence of tumor heterogeneity in large tumors. Our analyses examined blood and glucose metabolism in the most metabolically active portion of the tumor as indicators of the "worst-case" tumor behavior. Methods for assessing tumor heterogeneity, such as parametric imaging using mixture analysis (*35*), may provide additional insights into tumor biology.

In our previous work, we have shown that various blood flow and glucose metabolism patterns are predictive of response to chemotherapy. Measuring both blood flow and glucose metabolism parameters at the same time provided more insight into tumor biology than either alone. We have now extended this work with a more detailed analysis of tumor ^{18}F-FDG kinetics and found that the residual K_i/K_1 after 2 mo of chemotherapy was predictive of pathologic response. One advantage of this ratio is that the data can be obtained from 1 single dynamic ^{18}F-FDG study rather than 2 dynamic studies using ^{18}F-FDG and ^{15}O-water. This can circumvent the use of ^{15}O-water, which is only available in centers with an on-site cyclotron. We also showed that K_1 and blood flow are correlated both before and after therapy in accord with reports by Zasadny et al. (*11*). K_1 may therefore be a suitable substitute for blood flow for some aspects of the analysis.

Future studies will further explore biologic mechanisms underlying our findings by examining other tumor biologic factors that may affect response and lead to alterations in blood flow and metabolism. This will involve other imaging measures of in vivo tumor biology as well as in vitro assay of gene products that affect tumor metabolism and blood flow, such as hypoxia-inducible factor 1 and vascular endothelial growth factor (*32*). As outcome data become available, additional analysis will be performed to assess the predictive capabilities of the kinetic parameters.

CONCLUSION

Chemotherapy alters the pattern of glucose metabolism in LABC as evidenced by a change in the relationship among ^{18}F-FDG rate parameters with each other and with tumor blood flow. ^{18}F-FDG metabolism and blood flow appear to be more closely matched after chemotherapy than in untreated tumors. This finding can be explained in part by a decrease in the ratio of tumor metabolism to blood flow to levels closer to those of the normal breast tissue, suggesting that tumors shift to more aerobic glycolysis after chemotherapy. Observing changes in the pattern of glucose metabolism relative to blood flow may be useful for assessing response to chemotherapy and may provide insight into the variability of tumor response.

ACKNOWLEDGMENTS

The authors thank Drs. Julie Gralow, Georgiana Ellis, Hanna Linden, Robert Livingston, and the staff at the University of Washington Breast Cancer Specialty Clinic for collaboration and patient referrals; Dr. Thomas Lawton for assistance with pathology interpretations; Joanne Wells for modeling assistance; David Truong for providing Kinetic Imaging System software; and Dr. Kenneth Krohn for helpful comments. This work was supported by National Institutes of Health grants CA72064 and CA42045. Stipend support was provided by the Department of Radiology, University of Washington.

REFERENCES

1. Beahrs OH. Staging of cancer. *CA Cancer J Clin.* 1991;41:121–125.
2. Hortobagyi GN. Comprehensive management of locally advanced breast cancer. *Cancer.* 1990;66:1387–1391.
3. Wahl R, Zasadny K, Helvie M, Hutchins G, Weber B, Cody R. Metabolic monitoring of breast cancer chemohormonotherapy using positron emission tomography: initial evaluation. *J Clin Oncol.* 1993;11:2101–2111.
4. Bassa P, Kim E, Inoue T, et al. Evaluation of preoperative chemotherapy using PET with fluorine-18-fluorodeoxyglucose in breast cancer. *J Nucl Med.* 1996;37:931–938.
5. Jansson T, Westlin JE, Ahlstrom H, et al. Positron emission tomography studies in patients with locally advanced and/or metastatic breast cancer: a method for early therapy evaluation? *J Clin Oncol.* 1995;13:1470–1477.
6. Smith IC, Welch AE, Hutcheon AW, et al. Positron emission tomography using [^{18}F]-fluorodeoxy-D-glucose to predict the pathologic response of breast cancer to primary chemotherapy. *J Clin Oncol.* 2000;18:1676–1688.
7. Schelling M, Avril N, Nahrig J, et al. Positron emission tomography using [^{18}F]fluorodeoxyglucose for monitoring primary chemotherapy in breast cancer. *J Clin Oncol.* 2000;18:1689–1695.
8. Mankoff DA, Dunnwald LK, Gralow JR, et al. Blood flow and metabolism in locally advanced breast cancer: relationship to response to therapy. *J Nucl Med.* 2002;43:500–509.
9. Mankoff DA, Dunnwald LK, Gralow JR, et al. Changes in blood flow and metabolism in locally advanced breast cancer treated with neoadjuvant chemotherapy. *J Nucl Med.* 2003;44:1806–1814.
10. Sokoloff L, Reivich M, Kennedy C, et al. The [^{14}C]deoxyglucose method for the measurement of local cerebral glucose utilization: theory, procedure, and normal values in the conscious and anesthetized albino rat. *J Neurochem.* 1977;28:897–916.
11. Zasadny KR, Tatsumi M, Wahl RL. FDG metabolism and uptake versus blood flow in women with untreated primary breast cancers. *Eur J Nucl Med Mol Imaging.* 2003;30:274–280.
12. Vaupel P, Briest S, Hockel M. Hypoxia in breast cancer: pathogenesis, characterization and biological/therapeutic implications. *Wien Med Wochenschr.* 2002;152:334–342.
13. Feldman LD, Hortobagyi GN, Buzdar AU, Ames FC, Blumenschein GR. Pathological assessment of response to induction chemotherapy in breast cancer. *Cancer Res.* 1986;46:2578–2581.
14. Lewellen TK, Kohlmyer S, Miyaoka R, Schubert S, Stearns C. Investigation of the count rate performance of the General Electric ADVANCE positron emission tomograph. *IEEE Trans Nucl Sci.* 1995;42:1051–1057.
15. Wilson CBJH, Lammertsma AA, McKenzie CG, Sikora K, Jones T. Measurements of blood flow and exchanging water space in breast tumors using positron emission tomography: a rapid and non-invasive dynamic method. *Cancer Res.* 1992;52:1592–1597.
16. Furler SM, Jenkins AB, Storlien LH, Kraegen EW. In vivo location of the rate-limiting step of hexose uptake in muscle and brain tissue of rats. *Am J Physiol.* 1991;261:E337–E347.
17. Beaney RP, Lammertsma AA, Jones T, McKenzie CG, Halnan KE. Positron emission tomography for in-vivo measurement of regional blood flow, oxygen utilisation, and blood volume in patients with breast carcinoma. *Lancet.* 1984;1:131–134.

18. Pendleton N, Pazouki S, Heerkens E, et al. Relationships between different measurements of vascularity and clinico-pathological parameters in breast cancer. *Anticancer Res.* 1998;18:4565–4568.
19. Fox SB, Leek RD, Weekes MP, Whitehouse RM, Gatter KC, Harris AL. Quantitation and prognostic value of breast cancer angiogenesis: comparison of microvessel density, Chalkley count, and computer image analysis. *J Pathol.* 1995;177:275–283.
20. Kohlmyer S, Vesselle H, Miyaoka R, Kaplan M, Lewellen T. Comparison of recovery coefficients for PET based on maximum and average ROI pixel values. Presented at: European Association of Nuclear Medicine Annual Meeting; 2000; Paris, France. Abstract OS.329.
21. Bland M. *An Introduction to Medical Statistics.* 3rd ed. Oxford, U.K.: Oxford University Press; 2000:200–201.
22. Phelps ME, Huang SC, Hoffman EJ, Selin C, Sokoloff L, Kuhl DE. Tomographic measurement of local cerebral glucose metabolic rate in humans with (F-18)2-fluoro-2-deoxy-D-glucose: validation of method. *Ann Neurol.* 1979;6:371–388.
23. Spence AM, Muzi M, Graham MM, et al. Glucose metabolism in human malignant gliomas measured quantitatively with PET, 1-[C-11]glucose and FDG: analysis of the FDG lumped constant. *J Nucl Med.* 1998;39:440–448.
24. Okazumi S, Isono K, Enomoto K, et al. Evaluation of liver tumors using fluorine-18-fluorodeoxyglucose PET: characterization of tumor and assessment of effect of treatment. *J Nucl Med.* 1992;33:333–339.
25. Torizuka T, Tamaki N, Inokuma T, et al. In vivo assessment of glucose metabolism in hepatocellular carcinoma with FDG-PET. *J Nucl Med.* 1995;36:1811–1817.
26. Fukunaga T, Okazumi S, Koide Y, Isono K, Imazeki K. Evaluation of esophageal cancers using fluorine-18-fluorodeoxyglucose PET. *J Nucl Med.* 1998;39:1002–1007.
27. Dimitrakopoulou-Strauss A, Strauss LG, Schwarzbach M, et al. Dynamic PET ^{18}F-FDG studies in patients with primary and recurrent soft-tissue sarcomas: impact on diagnosis and correlation with grading. *J Nucl Med.* 2001;42:713–720.
28. Schmidt K, Lucignani G, Moresco RM, et al. Errors introduced by tissue heterogeneity in estimation of local cerebral glucose utilization with current kinetic models of the [^{18}F]fluorodeoxyglucose method. *J Cereb Blood Flow Metab.* 1992;12:823–834.
29. Schelbert HR. PET contributions to understanding normal and abnormal cardiac perfusion and metabolism. *Ann Biomed Eng.* 2000;28:922–929.
30. Raichle ME. Behind the scenes of functional brain imaging: a historical and physiological perspective. *Proc Natl Acad Sci USA.* 1998;95:765–772.
31. Torizuka T, Zasadny KR, Recker B, Wahl RL. Untreated primary lung and breast cancers: correlation between F-18 FDG kinetic rate constants and findings of in vitro studies. *Radiology.* 1998;207:767–774.
32. Semenza GL. HIF-1 and tumor progression: pathophysiology and therapeutics. *Trends Mol Med.* 2002;8(4 suppl):S62–S67.
33. Knowles HJ, Harris AL. Hypoxia and oxidative stress in breast cancer: hypoxia and tumourigenesis. *Breast Cancer Res.* 2001;3:318–322.
34. Rathmell JC, Fox CJ, Plas DR, Hammerman PS, Cinalli RM, Thompson CB. Akt-directed glucose metabolism can prevent Bax conformation change and promote growth factor-independent survival. *Mol Cell Biol.* 2003;23:7315–7328.
35. O'Sullivan F. Imaging radiotracer model parameters in PET: a mixture analysis approach. *IEEE Trans Med Imaging.* 1993;12:399–412.

JNM The Journal of NUCLEAR MEDICINE

^{18}F-FDG Kinetics in Locally Advanced Breast Cancer: Correlation with Tumor Blood Flow and Changes in Response to Neoadjuvant Chemotherapy

Jeffrey Tseng, Lisa K. Dunnwald, Erin K. Schubert, Jeanne M. Link, Satoshi Minoshima, Mark Muzi and David A. Mankoff

J Nucl Med. 2004;45:1829-1837.

The Journal of Nuclear Medicine is published monthly.
SNMMI | Society of Nuclear Medicine and Molecular Imaging
1850 Samuel Morse Drive, Reston, VA 20190.
(Print ISSN: 0161-5505, Online ISSN: 2159-662X)

SNMMI SOCIETY OF NUCLEAR MEDICINE AND MOLECULAR IMAGING